Environmental Science and Pollution Research (2018) 25:36645–36660
https://doi.org/10.1007/s11356-018-3504-y

RESEARCH ARTICLE

Zinc incorporation in marine bivalve shells grown in mine-polluted seabed sediments: a case study in the Malfidano mining area (SW Sardinia, Italy)

Daniela Medas[1] · Ilaria Carlomagno[2,3] · Carlo Meneghini[2] · Giuliana Aquilanti[4] · Tohru Araki[5] · Diana E. Bedolla[4] · Carla Buosi[1] · Maria Antonietta Casu[6] · Alessandra Gianoncelli[4] · Andrei C. Kuncser[7] · V. Adrian Maraloiu[7] · Giovanni De Giudici[1]

Received: 31 July 2018 / Accepted: 16 October 2018 / Published online: 30 October 2018

Abstract

Zinc incorporation into marine bivalve shells belonging to different genera (*Donax*, *Glycymeris*, *Lentidium*, and *Chamelea*) grown in mine-polluted seabed sediments (Zn up to 1% *w*/*w*) was investigated using x-ray diffraction (XRD), chemical analysis, soft x-ray microscopy combined with low-energy x-ray fluorescence (XRF) mapping, x-ray absorption spectroscopy (XAS), and transmission electron microscopy (TEM). These bivalves grew their shells, producing aragonite as the main biomineral and they were able to incorporate up to 2.0–80 mg/kg of Zn, 5.4–60 mg/kg of Fe and 0.5–4.5 mg/kg of Mn. X-ray absorption near edge structure (XANES) analysis revealed that for all the investigated genera, Zn occurred as independent Zn mineral phases, i.e., it was not incorporated or adsorbed into the aragonitic lattice. Overall, our results indicated that Zn coordination environment depends on the amount of incorporated Zn. Zn phosphate was the most abundant species in *Donax* and *Lentidium* genera, whereas, *Chamelea* shells, characterized by the highest Zn concentrations, showed the prevalence of Zn-cysteine species (up to 56% of total speciation). Other Zn coordination species found in the investigated samples were Zn hydrate carbonate (hydrozincite) and Zn phosphate. On the basis of the coordination environments, it was deduced that bivalves have developed different biogeochemical mechanisms to regulate Zn content and its chemical speciation and that cysteine plays an important role as an active part of detoxification mechanism. This work represents a step forward for understanding bivalve biomineralization and its significance for environmental monitoring and paleoreconstruction.

Keywords Bivalve · Biomineralization · Detoxification · Synchrotron x-ray techniques · Trace metals · Zinc

Introduction

The anthropogenic activities can have a drastic impact on marine environments (Cherchi et al. 2012; Frau et al. 2015; Romano et al. 2017), as they can lead to the degradation of sea sediments (Salvi et al. 2015) and seafood quality (Bilgin and Uluturhan-Suzer 2017). In coastal areas, metals are derived from the natural erosion of the upstream basins and from

Responsible editor: Philippe Garrigues

Electronic supplementary material The online version of this article (https://doi.org/10.1007/s11356-018-3504-y) contains supplementary material, which is available to authorized users.

✉ Daniela Medas
dmedas@unica.it

[1] Department of Chemical and Geological Sciences, University of Cagliari, Cagliari, Italy

[2] Department of Sciences, University of Roma Tre, Rome, Italy

[3] Present address: Elettra-Sincrotrone Trieste, Basovizza, Trieste, Italy

[4] Elettra-Sincrotrone Trieste, Basovizza, Trieste, Italy

[5] Diamond Light Source, Diamond House, Harwell Science and Innovation Campus, Oxfordshire, Didcot, UK

[6] UOS of Cagliari, National Research Council, Scientific and Technological Park of Sardinia POLARIS, Institute of Translational Pharmacology, Pula, Italy

[7] Laboratory of Atomic Structures and Defects in Advanced Materials, National Institute of Materials Physics, Atomistilor 405A, Magurele, Romania

anthropogenic sources (Apitz et al. 2009; Morelli et al. 2017). Human activities comprise (i) modern or past mining/industrial activities (De Giudici et al. 2017, 2018a; Arfaeinia et al. 2016; Romano et al. 2017; Atzori et al. 2018) and (ii) special sources such as ballast waters (Soleimani et al. 2016; Dobaradaran et al. 2018b) and cigarette butts (Dobaradaran et al. 2017, 2018a). Marine bivalves are sensitive organisms that register environmental changes (Carroll and Romanek 2008; Hahn et al. 2012; Jou et al. 2016 and reference therein), and they help in assessing the effect of metal dispersion caused by anthropogenic activities (Boening 1999; Zuykov et al. 2013; Amoozadeh et al. 2014; Sarmiento et al. 2016; Wong et al. 2017). Moreover, bivalve shells are well represented in fossil records (Huanxin et al. 2000), resulting useful proxies for investigating into the past (Kastner 1999).

The ability of bivalves to accumulate trace metals and organic chemicals (Faggio et al. 2018) from the environment has been extensively studied in recent years (Lopes-Lima et al. 2012), as it represents a valuable information in the field of environmental sciences revealing details about biogeochemical interactions potentially useful for bioremediation purposes. Most of the previous studies focused on pollutant accumulation in soft tissues of bivalves from native specimens and/or transplanted specimens (Kucuksezgin et al. 2013; Rzymski et al. 2014), and showed that the soft parts of the organism are useful bioindicators in aquatic ecosystems (Andral et al. 2011; Guo and Feng 2018). Indeed, bivalve mollusks are filter-feeding organisms, able to concentrate in their soft tissues various contaminants from the ambient water, reaching concentrations several orders of magnitude higher than those of the ambient environment (Zuykov et al. 2013 and reference therein). Bivalve soft tissues can be used to assess environmental conditions over short time scales, whereas shells appear to be more sensitive to environmental changes over the long term (Koide et al. 1982; Brown et al. 2005; Vaughn 2018). Incorporation of metals in bivalve shells (Carroll and Romanek 2008) is influenced by the biochemistry of the extrapallial fluid from which the shell is deposited (Wilbur and Saleuddin 1983), biological factors such as growth rate (Tevesz and Carter 1980; Stecher et al. 1996), and metabolic controls on shell formation (Rosenberg and Hughes 1991). In addition, water pH, temperature, salinity, availability of nutrients, metal contents (including contaminants), food availability, and population density affect the shell composition (Hahn et al. 2012; Zuykov et al. 2013).

To our knowledge, no previous investigations were performed on metal incorporation into bivalve shells collected along the Sardinian costs. Past literature mainly focused on metal accumulation in the soft tissues (Lafabrie et al. 2007; Schintu et al. 2008; Andral et al. 2011; Moschino et al. 2017; Sforzini et al. 2018), demonstrating an alteration of the health status of transplanted mussels in the contaminated sites. In this study, we explored bivalve shells collected along Buggerru and San Nicolò beaches (SW Sardinia, Italy), located near the Malfidano mining district (Zn and Pb mine of the Sulcis-Iglesiente area). This abandoned mining district is characterized by the presence of 2.6 million m^3 of open-pit excavations and 1.3 million m^3 of dump and tailings (RAS 2008), which have drastic effects on freshwater and marine environments. During the mining period, the residues were disposed in a tailing pond located on the coast. Periodically, the pond was opened to allow the disposal of new residues. In the late 1970s, the pond was removed with the opening of the dam, and the residues were dispersed into the sea through water jets (RAS 2008). Harmful metal contamination on the coastal area of Buggerru is a particularly important issue because of the potential threats of metal toxicity to the health of human residents. Furthermore, it can compromise tourism development. Romano et al. (2017) demonstrated the environmental impact of mining activity in marine sediments of the Sulcis-Iglesiente district, investigating marine sediment cores, and showed that Zn concentration reaches 14 g/kg. Although Zn was naturally enriched because of the outcropping of metal-based ores in the area, its anthropogenic enrichment was recognized, and it was mainly attributed to dispersion along the coast of mine waste material from the inland. The most abundant genera we found in the coastal area of the Malfidano mining district are *Donax*, *Glycymeris*, *Lentidium*, and *Chamelea*, both at Buggerru and San Nicolò.

Zn detoxification in bivalves is a well-known mechanism that can specifically occur via (i) Zn immobilization in Ca phosphate granules associated with digestive and excretory tissues (Coombs and George 1978; Brown 1982; Simkiss and Mason 1983; Deb and Fukushima 1999); (ii) Zn accumulation in membrane-limited vesicles associated with P (George et al. 1978); (iii) Zn deposition in the mineral structures (shell and/or microspherules; Pietrzak et al. 1976) and within the nacreous layer of the shell (Moura et al. 1999; Lopes-Lima et al. 2012). Previous studies on bivalve shells mainly focused on the mean metal content in whole shells (Steinhardt et al. 2016) and the shell pattern distribution of metals and its inter-shell variability (Tynan et al. 2005). A relationship was established between the metal content in the shells and the metal concentration in sediments and waters (Karbasdehi et al. 2016a, b; Cariou et al. 2017). To date, the coordination environment of Zn incorporated into the mineralized shell has not yet been investigated, though it represents a fundamental knowledge to assess the nature of Zn biomineral phases and the biological mechanism involved in the detoxification. Improvement in analytical techniques for accurate mineralogical and geochemical analyses, such as synchrotron x-ray techniques (De Giudici et al. 2014a; Luo and Zhang 2010; Medas et al. 2014b; Castillo-Michel et al. 2017) and the possibility to combine several complementary state of art probes promises to document chemical distribution and speciation of trace elements in biogenic minerals (Medas et al. 2017a, 2018).

In this work, we specifically addressed the question of S and trace element incorporation, in particular Zn and Fe, in the carbonate shells of Malfidano area combining laboratory and SR techniques, namely soft x-ray microscopy combined with low-energy x-ray fluorescence (XRF) mapping analysis, analytical transmission electron microscopy (TEM), and x-ray absorption spectroscopy (XAS) to achieve an effective multi-probe characterization of the same samples, obtaining an accurate and reliable understanding about the biomineralization process. Particularly, the aims of this work were (i) understanding if Zn is homogeneously incorporated and distributed across the shell, (ii) inferring if Zn correlates with other major and minor elements, and (iii) finding if the Zn speciation is unique or Zn can occur in multiple coordination environments. The results from this study will be also useful to develop biomonitoring techniques and to elucidate the impact of metals along the trophic chain in mine-polluted shoreface sediments (De Giudici et al. 2018b). Further studies will be devoted to investigate speciation of other metals.

Study area

The study was conducted in the Malfidano area, located in the Iglesiente mining district (SW Sardinia, Fig. 1). The deposits are mainly Paleozoic formations, which are represented by Cambrian–Ordovician rocks. The Lower Cambrian successions comprise siliciclastic sedimentary rocks and carbonate intercalations (Nebida group) as well as shallow water platform carbonate rocks (Gonnesa Gropus; Bechstädt and Boni 1994). The Middle and Upper Cambrian–Lower Ordovician successions are represented by nodular limestones and slates of Campo Pisano Formation and Cabitza Formation (Iglesias Group), respectively. The Quaternary deposits consist of eolian dunes along the coast and fluvial deposits in the internal area.

Ore deposits were exploited from 1870 to 1980 and they consisted both of primary sulfides, related to the metamorphism and magmatism that occurred during the Variscan Orogeny (Marcello et al. 2004) and calamine deposits. In the Iglesiente mining district, the primary sulfides occurred in massive, columnar, lens- and vein-like shapes in the carbonatic formations, and included sphalerite (ZnS) and galena (PbS) with a normal Zn grade of about 8–12 wt% (Marcello et al. 2004). The calamine deposits were derived from different weathering episodes that occurred within the Dolomia Gialla (hydrothermal Dolomia Geodica). Smithsonite and hemimorphite were the principal Zn-bearing minerals associated with nodules of remnant or supergene galena and sphalerite (Stara et al. 1996; Boni et al. 2003), with an overall Zn grade exceeding 20–22 wt% (Marcello et al. 2004).

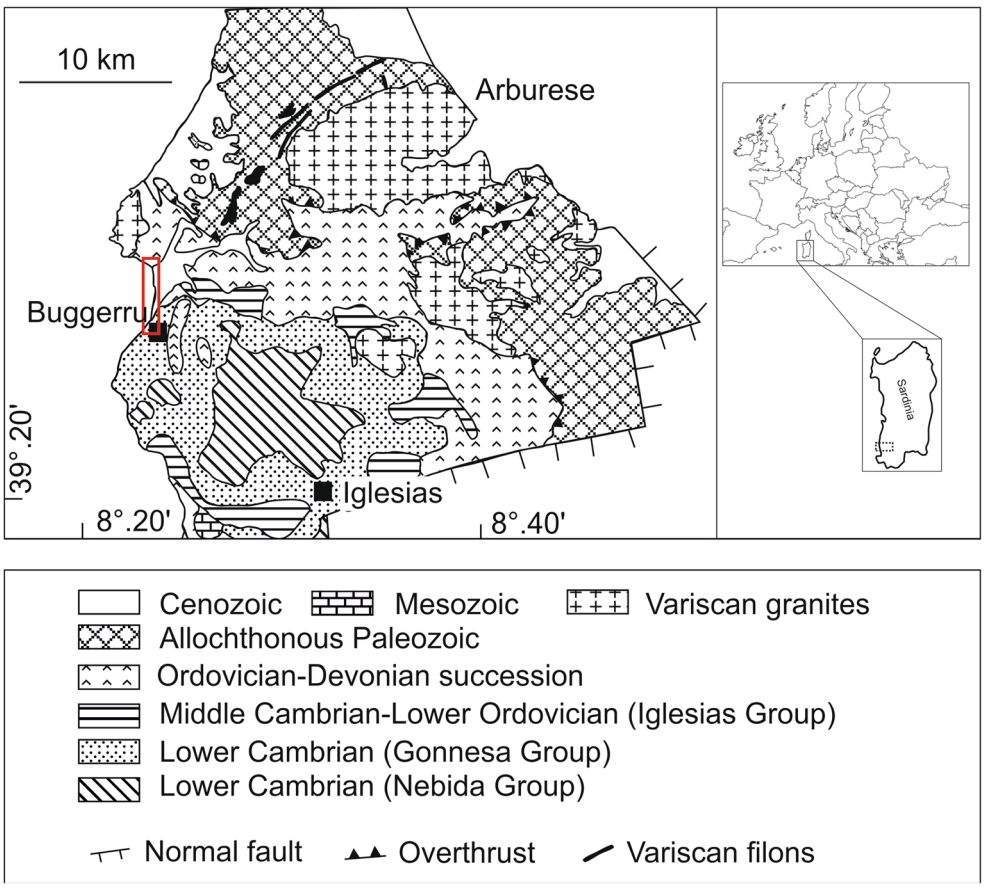

Fig. 1 Schematic geological map of the investigated area (Boni et al. 2003, modified). The red rectangular indicates the sampling area

Sample collection and methods

Bivalve samples of approximately similar shell sizes were collected handly from surface sediments along Buggerru and San Nicolò beaches (Fig. 2) on June 2016. The most abundant genera we found are *Donax*, *Glycymeris*, *Lentidium*, and *Chamelea* both at Buggerru and San Nicolò. At least 50 specimens for each genus were collected at each beach, immediately stored in bags, and transported to the laboratory. About 20 specimens per genus for each beach were selected, polled into one sample, and pulverized for mineralogical and chemical analysis.

Mineralogical and chemical analysis

Shell samples were initially washed in a laboratory under a gentle jet of deionized water and were gently brushed in ultrapure water with a nylon toothbrush to eliminate algae, sand, and other impurities. Shells were then washed several times in Milli-Q water and dried at room temperature for 1 week. Samples were grounded in an agate mortar and analyzed by x-ray diffraction (XRD) using laboratory θ–2θ equipment (Panalytical) with Cu Kα radiation ($\lambda = 1.54060$ Å), operating at 40 kV and 40 mA, and an X′celerator detector.

About 20 of similar-sized individuals of different bivalve species and same genus from each sampling site were used to avoid differences in metal content because of size, and they were grounded together to form one composite sample. Acid digestions were performed by EPA method 3050 with slight modifications according to Conners et al. (1999) on 0.5 g of each ground sample by adding 5 ml of concentrated superpure nitric acid (65–69%, Carlo Erba) at 90 °C in a hot plate for 2 h. Then, 3 ml of hydrogen peroxide (30% *w*/*w*, Sigma-Aldrich) were added to remove any remaining organic material at 90 °C for 1 h. Samples were processed together with blanks prepared with the same mixture to evaluate contamination from the reagents and sample containers. Finally, samples were filtered (0.4 μm) and the solutions were diluted to a final volume of 25 ml using Milli-Q water. Sulfur and metal concentrations (Zn and Fe) were quantified by inductively coupled plasma optical emission spectrometry (ICP-OES, ARL Fisons ICP Analyzer 3520 B), and inductively coupled plasma mass spectrometry (ICP-MS, PerkinElmer, Elan 5000/DRC-e, USA; Zn, Fe, Pb, Mn, Ni, Co, Cr, Cu, Cd, Se, Mo, As, Sb, and U). Trace elements not shown are below the limit of quantification (Cu < 0.1 mg/kg, Cr < 0.7 mg/kg, Se < 0.1 mg/kg, Mo < 0.1 mg/kg, As < 0.5 mg/kg, Sb < 0.05 mg/kg). In this work, we focused on S, Zn, and Fe incorporation because (i) they are important mineral components involved in biological reactions but an exposure to high concentrations of Zn and Fe may lead to variation in the properties of the bivalve shell (Hahn et al. 2012; Zuykov et al. 2013) and (ii) Zn and Fe are among the most abundant contaminants in the investigated area (Cidu et al. 2007, 2009).

Two duplicate samples were analyzed to estimate method precision (expressed as standard deviation/mean concentration) that was in the range 3–7% for Fe, 0.1–0.3% for Pb, 0.3–2% for Mn, 8–10% for Ni, 1–4% for Co, 2–4% for Ag, 2–5% for Cd, and 0.3–1% for U. The limits of detection (LOD) and of quantification (LOQ) are reported in Table 1. To evaluate the analytical accuracy of the acid digestion procedure, experimental values and the certified values of the reference material (BCS No. 368 - dolomite) were compared, and the percentage recovery (Table S1) of each metal was calculated as:

$$\%\text{Recovery} = \frac{\text{Mean value of the measured concentration } \left(\frac{\mu g}{l}\right)}{\text{Certified concentration } \left(\frac{\mu g}{l}\right)} \times 100$$

To estimate potential contaminations, the accuracy and precision of trace element analysis, procedural blanks, and

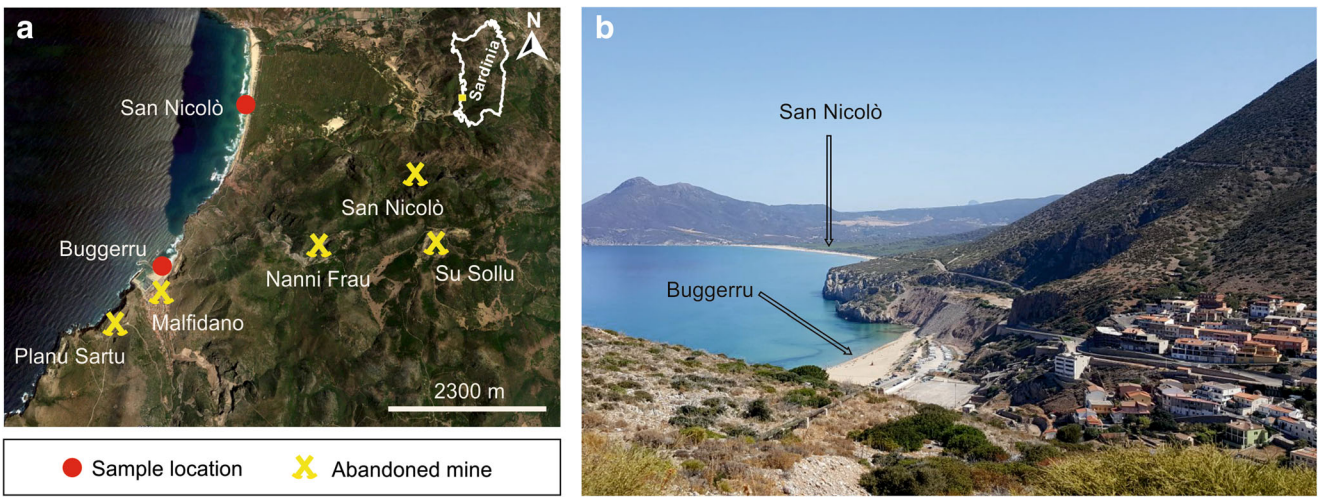

Fig. 2 Map of the sampling area. Image from Google Earth, modified (**a**). Photo of the sampling area (**b**)

Table 1 Sulfur and trace element concentration in bivalve shells. Precision, expressed as standard deviation/mean concentration of reference solution, < 5%. *Chamelea* and *Donax* from San Nicolò were digested in duplicate, the mean concentrations of each element are reported (precision 0.1–10%)

Sample	Locality	S mg/kg	Zn mg/kg	Fe mg/kg	Pb mg/kg	Mn mg/kg	Ni mg/kg	Co mg/kg	Cd mg/kg	U mg/kg
Donax	San Nicolò	1850	2.5	10	130	1.4	0.57	0.32	< 0.01	0.27
Glycymeris	San Nicolò	2000	2.0	60	180	1.3	0.63	0.32	< 0.01	0.25
Lentidium	San Nicolò	1900	3.6	10	110	2.0	0.6	0.3	< 0.01	0.21
Chamelea	San Nicolò	1950	8.3	20	80	2.0	0.6	0.31	0.03	0.3
Donax	Buggerru	1960	30	7.7	350	1.7	0.57	0.31	0.19	0.17
Glycymeris	Buggerru	2060	9.0	5.4	110	0.5	0.6	0.33	0.04	0.15
Lentidium	Buggerru	1950	30	20	100	2.0	0.58	0.3	0.21	0.19
Chamelea	Buggerru	2250	80	30	100	4.5	0.62	0.33	0.46	0.39
LOD*		3.0	0.06–0.3	0.1–0.4	0.01	0.1	0.02	0.005	0.05	0.005
LOQ*		10	0.2–1.0	0.4–1.3	0.02	0.3	0.07	0.01	0.01	0.02

*For S, LOD, and LOQ refer to ICP-OES; for Zn and Fe, values of LOD and LOQ are reported for ICP-MS and ICP-OES; for Pb, Mn, Ni, Co, Cd, and U, values of LOD and LOQ refer to ICP-MS

standard and reference solutions (SRM 1643e and EnviroMAT Drinking Water, High EP-H-3 and Low EP-L-3) were analyzed after every five samples.

X-ray microscopy techniques

Soft x-ray microscopy, low-energy XRF mapping, and TEM microscopy techniques were employed to investigate specific metal distributions from the micro- to the nanoscale. Iron and Zn distribution was investigated by soft x-ray microscopy combined with low-energy XRF mapping analysis. Sections of shell samples were prepared by dehydration in a graded series of acetone solutions (25, 50, 75, and 100%) followed by 100% toluol. All steps were carried out at room temperature for 15 min each. The samples were then left overnight in a mixture of 50:50 toluol/epon resin (Epon 812) followed by immersion in 100% resin for 30 min at room temperature, and then polymerization at 60 °C for 48 h. Semi-thin sections (1 μm) were cut with a diamond knife on ultramicrotome and collected on ultralen films. The analysis were performed at the TwinMic beamline (Gianoncelli et al. 2016a, b; Kaulich et al. 2006) at Elettra-Sincrotrone Trieste (Trieste, Italy).

The TwinMic microscope was operated in the scanning transmission x-ray microscope (STXM) mode, where the sample is scanned across a microprobe delivered by a suitable zone plate diffractive optics. Absorption and phase contrast images are generated from the transmitted x-rays (Gianoncelli et al. 2006; Morrison et al. 2006) collected through a fast readout charge-coupled device camera (Andor Technology), while the simultaneous XRF signals emitted by the specimen is acquired by eight silicon drift detectors (Gianoncelli et al. 2009, 2013). This setup allows the simultaneous collection of morphological and chemical information.

STXM data were mainly addressed to individuate the Fe and Zn distribution in the shell with micrometer resolution, the x-ray beam energy was 1.5 keV, to ensure the best excitation and detection of Zn and Fe, with a spatial resolution (x-ray spot size) of $1.2 \times 1.2\ \mu m^2$ as a compromise between a good XRF signal and dimension of the features of interest. The XRF elemental maps were deconvoluted and analyzed with PyMCA software (Solé et al. 2007).

TEM analysis provided elemental distribution with subnanometric resolution. The shell samples for TEM analysis were gently crushed in an agate mortar and dispersed in ultrapure water in an ultrasonic bath for 3 min. A droplet of this suspension was then deposited onto a TEM Cu grid. For analytical scanning TEM (STEM) investigations, we used a JEOL 2100 microscope (NIMP, Laboratory of Atomic Structures and Defects in Advanced Materials, Magurele, Romania) equipped with a LaB_6 gun and JEOL JED-2300T energy-dispersive x-ray spectrometer. The acceleration voltage was 200 kV. Energy-dispersive x-ray spectroscopy (EDS) mapping in STEM mode was performed to map the distribution of the main component elements in the samples (Zn, Fe, Ca, and S). This technique provides simultaneously both spatial and spectral information in each acquired pixel. A selected area was scanned using a convergent beam with a diameter of approximately 0.3 nm, and the x-ray signal from each point of the scan was collected by the detector.

Calcium and S distribution was further investigated by scanning transmission x-ray microscopy (STXM) combined with XRF elemental mapping analysis at the I08-SXM beamline in Diamond Light Source, Didcot, UK. Sections of shell samples were selected and prepared using the same procedure for the TwinMic beamline and fixed on silicon nitride thin membranes. The x-ray beam was focused down to about 800 nm with a tungsten Fresnel zone plate (40-nm outermost zone width and

333-um diameter) optimized to ensure a good XRF sensitivity with a compromised spatial resolution for this work. X-ray fluorescence mapping was conducted using a 4.1-keV photon energy to collect the Ca K-edge fluorescence, and simultaneously, transmission images were recorded with a photo diode. Preliminary S K-edge x-ray absorption near edge structure (XANES) spectromicroscopy data were collected to speciate the S chemical states of the *Chamelea* sample. Quantitative STXM data analysis and element mapping were performed using MANTiS (Lerotic et al. 2014) and PyMca (Solé et al. 2007), respectively.

Correlation analysis

In order to evaluate the relative distribution of selected elements in the shells, the linear correlation $\rho_{A\text{-}B}$ between the fluorescence intensities of A and B elements in the maps was calculated (De Giudici et al. 2018b). Higher correlation values point out major co-localization of the A and B elements in the maps, lower correlation suggests the A and B elements are in different regions of the shells, thus in different phases. The correlation analysis was carried out using a python script based on the Numpy (2014) and Scipy (2014) libraries. The script may use a cutoff intensity value to automatically individuate voids in the images and select only the image regions corresponding to shell regions. Noticeably, the correlation estimate is affected by statistical noise on pixel intensity (Poisson counts); in EDS TEM images, the counts per pixel in the energy region of interest (ROI) may be quite low, even close to the unit, giving high Poisson noise that may reach the 50% of the signal, worsening the correlation estimate. In order to reduce the statistic noise, the script allows integrating ROI counts over $N \times N$ pixel squares. We selected $N = 4$ in the EDS TEM correlation analysis, while $N = 1$ is used for analysis of STXM images.

X-ray absorption spectroscopy at the Zn K-edge

X-ray absorption spectroscopy (XAS) measurements were carried out at the Zn K-edge (9.659 keV) at the x-ray absorption fine structure (XAFS) beamline of Elettra-Sincrotrone Trieste (Trieste, Italy; Di Cicco et al. 2009) with the aim to individuate the chemical nature of Zn species in the shells. The cleaned shell samples were ground and mixed with polyvinyl pyrrolidone (PVP) matrix (2:1 weight ratio), then pressed in thin solid pellets suitable for XAS measurements. The Zn K-edge absorption spectra were measured in fluorescence geometry at room temperature. Reference materials, including inorganic and organic materials (Table 2 and Fig. S1), were measured in transmission geometry and used for XANES interpretation by linear combination analysis (LCA; Benfatto and Meneghini 2014). Zn K-edge raw XAS data were treated following the standard methods (Meneghini et al. 2005, 2012) for background subtraction and edge-jump normalization. The XAS data have been analyzed in the near-edge region (XANES), using a set of reference compounds (Table 2) for the LCA (Torchio et al. 2010). Because the relatively low Zn concentration in the shells and the complex average Zn coordination (see LCA), the quantitative analysis of the extended EXAFS signal cannot provide further details.

Results

Mineralogical composition and trace metals concentration

Figure 3 shows the XRD pattern of the bivalve shells. All the investigated genera produce mainly aragonite biomineralization. Trace element concentrations in the bivalve shell are reported in Table 2. The most abundant metals were Zn (2.0–80 mg/kg), Fe (5.4–60 mg/kg), Pb (80–350 mg/kg), and Mn (0.5–4.5 mg/kg), having an ample concentration variability in all the analyzed samples. Nickel and Co showed less variable contents, ranging from 0.57–0.65 mg/kg and 0.30–0.33 mg/kg, respectively. Noticeably, S concentration is the highest, ranging from 1950 to 2250 mg/kg, similar among the investigated samples. Looking at the metal concentrations (Table 2), we found that the variability of Zn content as a

Table 2 Reference compounds analyzed by x-ray absorption spectroscopy

No.	Name	Formula
1	Sphalerite	ZnS
2	Smithsonite	$ZnCO_3$
3	Hydrozincite	$Zn_5(CO_3)_2(OH)_6$
4	Willemite	Zn_2SiO_4
5	Hemimorphite	$Zn_4Si_2O_7(OH)_2{\cdot}H_2O$
6	Zn oxide	ZnO
7	Zn sulphate monohydrate	$ZnSO_4{\cdot}H_2O$
8	Zn sulphate heptahydrate	$ZnSO_4{\cdot}7H_2O$
9	Zn calcite solid solution	Zn in $CaCO_3$
10	Zn adsorbed on calcite	Zn in $CaCO_3$
11	Zn phosphate	$Zn_3(PO_4)_2$
12	Zn in hydroxyapatite	Zn in $Ca_5(PO_4)_3(OH)$
13	Zn acetate dehydrate	$Zn(O_2CCH_3)_2(H_2O)_2$
14	Zn acetate anhydrous	$Zn(O_2CCH_3)_2$
15	Zn citrate	$Zn_3(C_6H_5O_7)_2$
16	Zn malate	$ZnC_4H_6O_5$
17	Zn histidine	$ZnC_6H_9N_3O_2$
18	Zn cysteine	$ZnC_3H_7NO_2S$

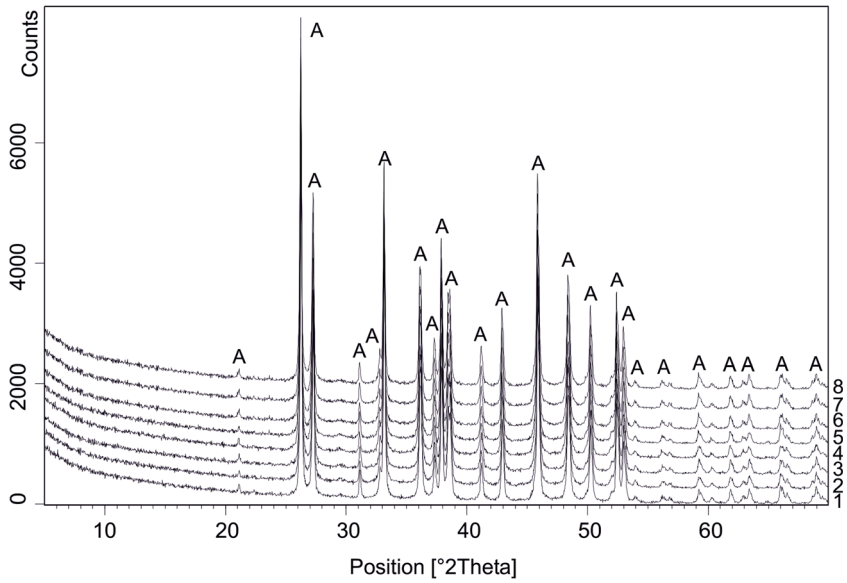

Fig. 3 XRD patterns of bivalves *Donax*, *Glycymeris*, *Lentidium*, and *Chamelea* collected along Buggerru (1, 2, 3, and 4) and San Nicolò beaches (5, 6, 7, and 8). A = aragonite

function of genus is strongly correlated ($r = 0.98$, $p = 0.02$), suggesting the Zn concentration in bivalve shells could be a genus-dependent parameter.

Elemental distribution

Selected representative STXM-XRF images (TwinMic and I08-SXM instruments) of thin cross sections from the central part of the shells are shown in Figs. 4 and 5, these provide selected element distribution with micrometer resolution (Table 3). Zinc and Fe were found weakly correlated to Ca ($\rho_{Zn\text{-}Ca} = 0.23$, $\rho_{Fe\text{-}Ca} = 0.08$), pointing out that Zn and Fe were not homogeneously dispersed in the aragonite matrix but may likely form Fe/Zn rich specific phases (De Giudici et al. 2018b). Moreover, Zn and Fe were also weakly correlated ($\rho_{Zn\text{-}Fe} = 0.09$–$0.15$) likely meaning they are located in different phases. The relatively high Ca–S correlation ($\rho_{Ca\text{-}S} = 0.47$) suggested that S is more homogeneously dispersed into the aragonite structure and preliminary μ-XANES investigation at the S K-edge showed that S was mainly present as sulfate (unpublished data) according to Yoshimura et al. 2013.

TEM image (Fig. 6a) shows a fragment with irregular shape and diameter of ~ 600 nm. The corresponding selected area-electron diffraction (SAED) pattern (Fig. 6b) demonstrates that the fragment had the aragonite crystalline structure (ICSD card no. 034308). EDS mapping (Fig. 6c, d) of aragonitic grain fragments provides elemental distribution details with nanometric spatial resolution. EDS images show that S and Ca are collocated in the shell ($\rho_{Ca\text{-}S} = 0.52$) accordingly to STXM-XRF analysis. Zinc and Fe are widely distributed in the shell, and Fe also can occur as concentrated spots (see arrows, Fig. 6c, d). Zinc and Fe clusters are evident in different regions (Fig. 6), explaining the low correlation coefficient ($\rho_{Zn\text{-}Fe} = 0.12$). The Fe ($\rho_{Fe\text{-}Ca} = 0.29$) and Zn ($\rho_{Zn\text{-}Ca} = 0.28$) correlation with Ca is weak, confirming at the nanometric scale the presence of Fe/Zn rich specific phases.

If the incorporation of Zn or Fe is mediated by a given element, then their abundance should be higher around the sites of this element. In this case, a high spatial correlation is expected between the intensity of this element and that of Zn or Fe. The inhomogeneous distribution of Zn across each map results in generally low Zn–Ca correlations. In the b1 region (Fig. 4), the highest Zn concentration is observed in small clusters located at the very bottom of the map. Away from this area, the Zn appears rarely co-located with Fe in some regions (left-hand side in the map), whereas it is almost absent where most of the Fe is observed (top right area in the map). This inhomogeneity results in the above-mentioned weak Zn–Fe correlation. In b2 and d4 (Fig. 4), the Zn–Fe correlation is slightly higher (up to $\rho_{Zn\text{-}Fe} = 0.25$) and can be visually predicted from the maps, this seems related to higher Fe concentration in these regions. In the sample of Fig. 4d, the Zn–Fe ratio is rather higher compared to the one observed in Fig. 4b. Furthermore, while Fe is more evenly spread on the surface, Zn appears to be mostly localized in small areas.

Zinc chemical environment in the aragonitic shells

XANES analysis provides details on Zn average valence state and coordination chemistry. Here, Zn speciation in bivalve shells was investigated by XANES analysis in samples having the highest Zn concentration (*Lentidium*, *Donax*, and *Chamelea* from Buggerru). We selected an ample set of reference compounds, both inorganic and organic (Table 2, Fig. S1). Figure 7 presents Zn XANES spectra of bivalve shells and a selected subset of relevant reference compounds. The

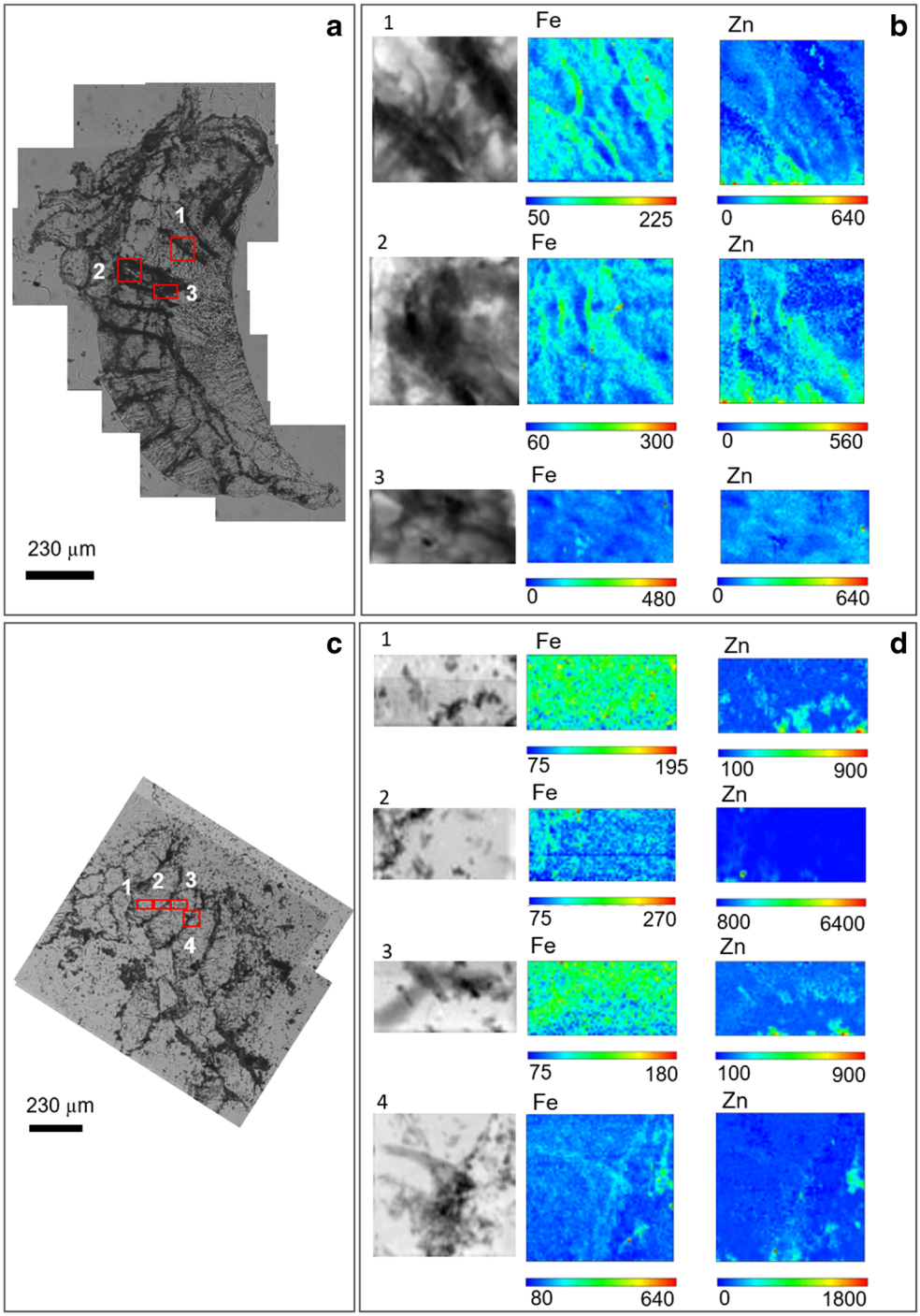

Fig. 4 Selected samples of *Glycymeris* collected at San Nicolò (**a**, **b**) and *Donax* collected at Buggerru (**c**, **d**). Ordinary light stereo-microscope image with the location of the acquired maps (**a**, **c**); bright field (absorption) images and LEXRF maps of Zn and Fe (**b**, **d**). Maps 1 and 2 of *Glycymeris*, size 80 × 80 μm^2, scan 64 × 64 pixels; map 3 of *Glycymeris*, size 80 × 40 μm^2, scan 64 × 32 pixels. Maps 1, 2, and 3 of *Donax*, size 80 × 40 μm^2, scan 64 × 32 pixels; map 3 of *Donax*, size 80 × 80 μm^2, scan 64 × 64 pixels

Zn K-edge XANES spectral features of bivalve samples show that Zn is incorporated as Zn^{2+} ions in the shells. The XANES spectral features are smoother and broader respect to the reference compounds (Fig. 7), likely due to several Zn phases and a more structurally disordered Zn environments in the shell samples. Comparing the Zn XANES spectral features of bivalve samples with those of the reference compounds, the similarity with the Zn phosphate spectrum is clear (Fig. 7, labels A–D). Specifically, the XANES features, labeled as A at the Zn phosphate edge white line, and the minimum labeled as D, were present in the bivalve spectra. In addition, the spectral features labeled as B and C in the Zn phosphate spectrum (Fig. 7) agreed with the spectral features observed in all the bivalve spectra.

Linear combination analysis (LCA) of XANES spectra (Benfatto and Meneghini 2014) was performed to determine

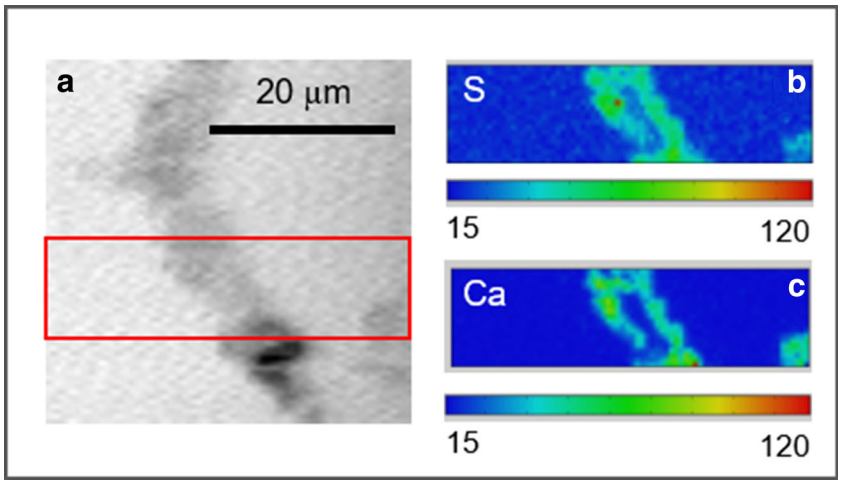

Fig. 5 Transmission image (**a**) and XRF maps of *Chamelea* (**b**, **c**) collected at I08 during SP16496 experiment with pixel size of ca. 800 nm. Ca K and S K-edges fluorescence signals are co-located in the section cut perpendicular to the shell

the main Zn phases present in these bivalve samples. We selected the reference spectra for the LCA from the compounds reported in Table 2. We followed a trial and error procedure based on a statistical analysis of the best fit residue (χ^2 test and *F* test) to determine the components giving the best agreement. Results are shown in Fig. 8. We found that in *Lentidium* and *Donax* the main contribution came from the Zn phosphate, followed by hydrozincite and Zn cysteine in the same amount. On the other hand, in *Chamelea*, Zn cysteine was the most abundant Zn specie, followed by Zn phosphate and hydrozincite (Fig. 9).

Discussion

Bivalve shells are built by a biologically controlled process occurring at the interface between the cells and the environment, resulting in an organo-mineral biocomposite, of which the Ca-carbonate mineral makes up 95–99% (Weiner et al. 1976; Lowenstam and Weiner 1989; Arivalagan et al. 2017). Aragonite and calcite dominate the mineral composition of the bivalve shells, which may wholly be aragonitic or contain both aragonite and calcite in separate monomineralic layers (Taylor et al. 1969). Calcite was found in the outer layer of superfamilies belonging to the subclass Pteriomorphia, excluding two species from the Heterodont superfamily Chamacea. (Kennedy et al. 2008). The remaining two superfamilies, the Arcacea and Limopsacea, have wholly aragonitic shells (Taylor et al. 1969). The organic and inorganic constituents are secreted by the cells into the extrapallial fluid (EPF) that lies in the extrapallial cavity between mantle and shell (Kennedy et al. 2008). The calcium used to build the shell is taken from the diet or seawater. Carbonate is derived from the CO_2/bicarbonate pool in the tissues of the animal (Lutz 2004).

The bivalve shell consists of three layers (Lutz 2004; Marin et al. 2012): a thin outer periostracum of horny conchiolin, a middle prismatic layer, and an inner nacreous layer. The periostracum is a quinone-tanned unmineralized protein layer that covers the external surface of the shell, enhancing abrasion resistance, and acting as barriers against predation (Yao et al. 2014), and it provides a nucleation site for calcium carbonate (Checa 2000). The prismatic layer grows below the periostracum (Yao et al. 2014) and it is secreted by the outer mantle fold. The calcite or aragonite prismatic layer contains

Table 3 Elemental intensity correlation (Pearson) from STXM-XRF and TEM-EDS images analysis (see text). Values are averaged over several images, uncertainties are estimated around 5–10%

Genus	Resolution	Element intensity correlation, $\rho_{A\text{-}B}$					
		Zn–Fe	Zn–Ca	Zn–S	Fe–Ca	Fe–S	Ca–S
Donax[a]	1.2 × 1.2 μm^2	0.12	–	–	–	–	–
Glycymeris[a]	1.2 × 1.2 μm^2	0.15	–	–	–	–	–
Chamelea[b]	0.8 × 0.8 μm^2	0.09	0.23	0.13	0.08	0.02	0.47
Chamelea[c]	0.3 × 0.3 nm^2	0.12	0.28	0.16	0.29	0.18	0.52

[a] TwinMic

[b] I08-SXM

[c] NIMP

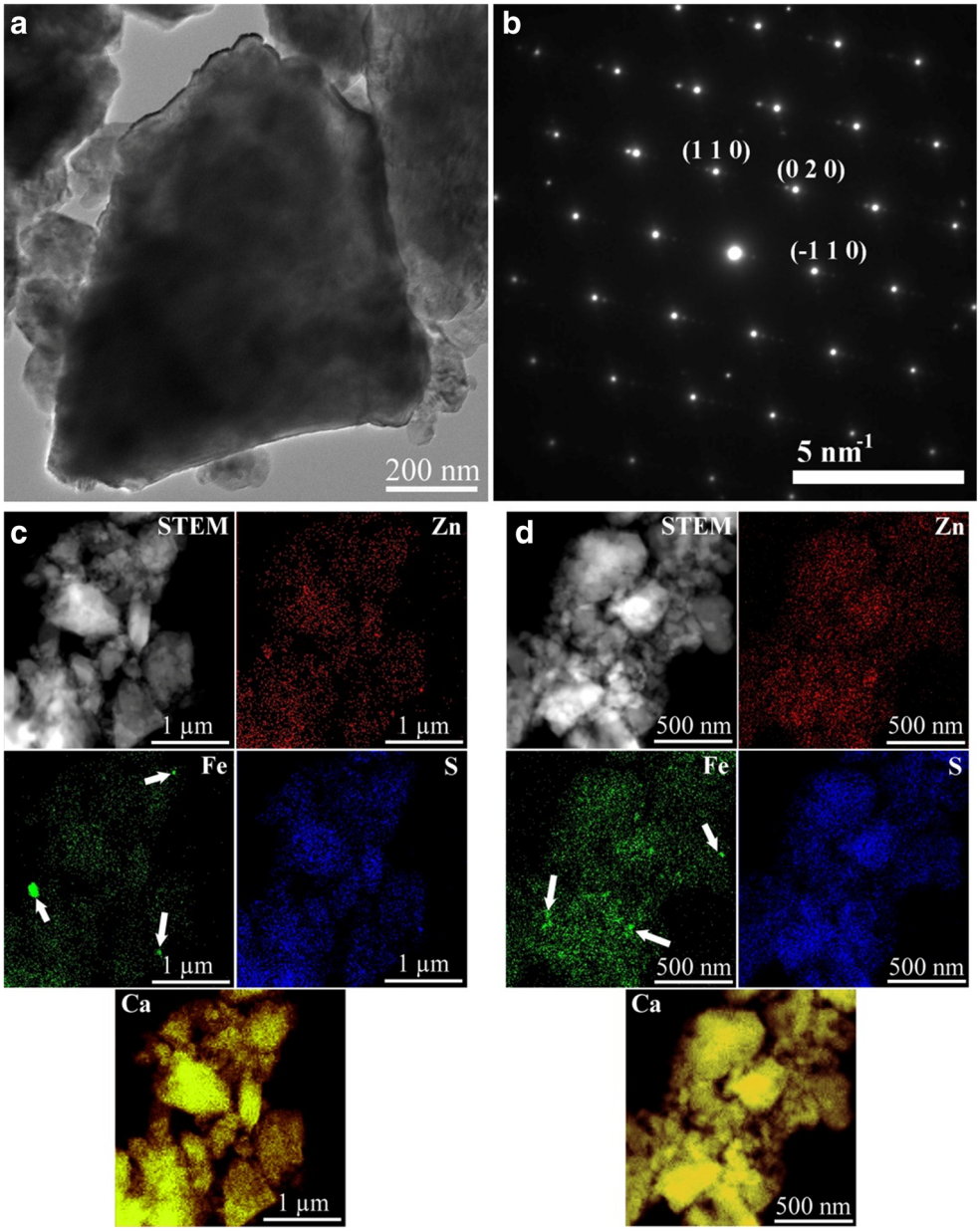

Fig. 6 TEM image (**a**) and the corresponding SAED pattern (**b**) of a fragment from *Chamelea* from Buggerru; **c**, **d** STEM images with the EDS maps (in false colors) of Zn, Fe, S, and Ca. White arrows indicate Fe-concentrated spots

organic matrices consisting of chitin (Suzuki et al. 2007) and proteins (Suzuki et al. 2004; Tsukamoto et al. 2004; Kong et al. 2009). Finally, the nacreous layer is deposited on the outer prismatic layer (Yao et al. 2014) by the general mantle surface (Lutz 2004). It is a micro-laminate composite material with highly oriented aragonite crystals. The organic matrix consists of several macromolecules, polysaccharides, proteins, and glycoproteins, located in both intercrystalline and intracrystalline positions within the nacre and constitutes 1–5% of the nacre shell weight structure (Yao et al. 2014).

Trace elements are actively incorporated in bivalve shells (Klein et al. 1996; Gillikin et al. 2005; Yan et al. 2014); these elements enter the EPF through the epithelial mantle cells via intracellular or intercellular transport ways (Klein et al. 1996; Gillikin et al. 2005) and affect the bivalve shell trace elements content (Yan et al. 2014). Despite all this extensive available information, the speciation of Zn in bivalve shells has not been investigated in the literature. In this study, we analyzed bulk shells and identified three main different Zn phases (Fig. 9): (i) Zn phosphate, (ii) hydrozincite, and (iii) Zn cysteine, motivating the low Zn–Ca correlation. Complementary XRF images of thin sections from the central part of the shells and TEM images of the aragonite (nano)crystals allowed us to determine that Zn was mainly located in the bulk of the aragonite crystal matrix (Figs. 5 and 6).

We recognized a difference in Zn chemical environment as a function of Zn concentration: Zn phosphate was found to be the most abundant species in the shells with the lowest Zn

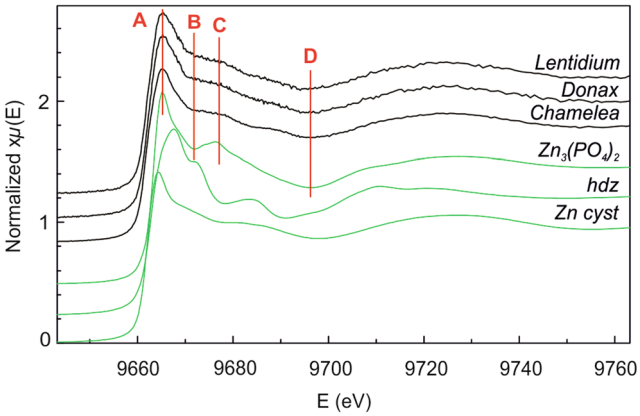

Fig. 7 XANES spectra at the Zn K-edge of *Lentidium*, *Donax*, and *Chamelea* collected at Buggerru and selected reference compounds: Zn phosphate ($Zn_3(PO_4)_2$), hydrozincite (hdz), and Zn cysteine (Zn cyst). Spectra are vertically shifted for clarity

content (*Lentidium*, with Zn concentration of 29 mg/kg and Zn_{phoph} of 51%; *Donax*, with Zn of 27 mg/kg and Zn_{phoph} of 55%). George et al. (1978) found that the detoxication of Zn by the oyster *Ostrea edulis* (L) takes place by Zn immobilization in membrane-limited vesicles associated with P. In our study, P also seems to be an excellent ligand in the aragonitic shells. This is confirmed by our correlation calculations, which shows a high Pearson's coefficient ($\rho_{Ca\text{-}P} = 0.54$). Furthermore, Zn cysteine became more relevant in *Chamelea*, characterized by higher Zn concentrations (80 mg/kg). It has been shown that cysteine-rich proteins have an important role in metal detoxification, as they act as metal-chelating agents for the excess metals in the soft parts of mollusks (Géret et al. 2002). Thus, we formulated a hypothesis that *Chamelea* genus has a higher fraction (56%) of Zn cysteine than *Lentidium* (24%) and *Donax* (23%) genera, indicating that cysteine synthesis in bivalve cellules increases when the Zn uptake from the organism is higher and the physiological response is the incorporation of excess of non-toxic Zn in the shell. Previous researches (Adediran et al. 2016) demonstrated that the coordination of metals with cysteine-rich peptides can occur in different organisms such as fungi (Ahmad et al. 2002), sulfate-reducing bacteria (Cunningham and Lundie 1993; Holmes et al. 1995). and plants growing in Zn-extreme environments (Medas et al. 2017b, 2015; Terzano et al. 2008; De Giudici et al. 2015; Adediran et al. 2016). Biomineral processes occurring in polluted environments were referred to as active detoxification mechanisms (Carney et al. 2007; Caldelas and Weiss 2017).

Hydrozincite can be recognized in marine shells only via chemical selective/local structure-sensitive techniques such as XAS (De Giudici et al. 2018b) because of the low concentration of Zn, owing to the characteristic features of the Zn K-edge spectra of hydrozincite. Hydrozincite extracellular biomineralization has been found to have an important role in cyanobacteria preservation (De Giudici et al. 2014b; Medas et al. 2013, 2014a; Podda et al. 2014), and recent studies from our group (De Giudici et al. 2018b) indicated that Zn can occur as a separate hydrozincite nanostructured phase in foraminifera shells grown in heavily Zn-polluted environment (Zn concentration in sediments exceeding 1% *w*/*w*), while distribution and crystallinity depend on specific cellular processes. To our knowledge, revealing a hydrozincite biomineralization in mollusk shells is completely novel. Noticeably, we found such hydrozincite phase in shells (foraminifera in a previous study and bivalves in the present study) grown in highly Zn-polluted sediments; this suggests that the hydrozincite formation must have a role in Zn incorporation/detoxification mechanisms. Current data do not allow us to assess if hydrozincite in mollusk shells forms because of specific cellular machinery

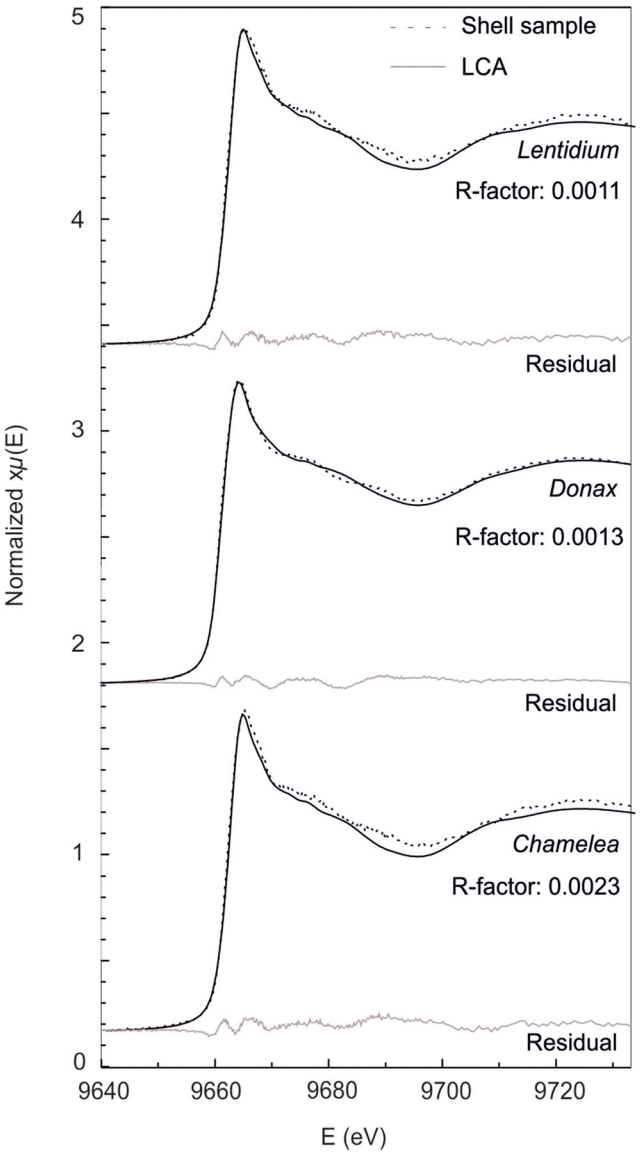

Fig. 8 Linear-combination analysis of the XANES spectra. The dashed lines are the experimental data, the solid lines are the fit, and the gray lines are the residue

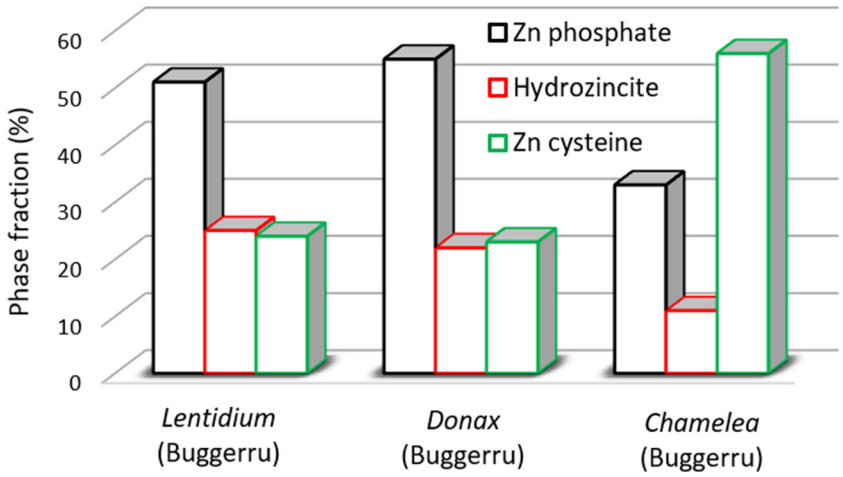

Fig. 9 Results of linear combination analysis of Zn XANES spectra. The sum of contribution fractions is fixed to 100%; the incertitude on the fraction values is around 5–8%

devoted to detoxification in heavily polluted environment or as a by-product of Ca-carbonate biological synthesis.

Theoretically, trace elements such as Mg, Sr, Zn, Mn, and Pb can substitute for the Ca^{2+} ion and thus become incorporated in the Ca-carbonate structure (Tynan et al. 2005). Previous researches (Soldati et al. 2016) found that, in different shells of freshwater bivalves, Mn was incorporated in the inorganic carbonate in the shell nacre of the internal region, and the structure of the aragonitic host was locally altered such that Mn attained an octahedral, calcitic coordination. The XANES analysis performed on the bivalve *Arctica islandica* indicated that Mg was not substituted into aragonite but was hosted by a disordered phase, e.g., organic components or nanoparticles of an inorganic phase (Foster et al. 2008), whereas Sr randomly substituted for Ca within the shell aragonite (Foster et al. 2009). In this study, Zn mainly occurred in independent Zn phases ($ZnPO_4$, Zn cysteine, and hydrozincite) being related to the synthesis of the shells. Thus, we argue that the Zn in our samples was not incorporated into the aragonite lattice or adsorbed onto the surfaces of Ca-carbonate (nano)crystals.

Conclusions

This study showed that bivalves can synthesize phases other than Ca-carbonate when exposed to high Zn concentrations. The elemental distribution analysis (STXM and TEM) suggested that Zn was incorporated as independent phases at the micrometric as well nanometric scale. Zn K-edge XANES chemical speciation demonstrated that these phases involved cysteine molecules, phosphate ions, and carbonate ions to regulate trace element concentration. The relative amount of Zn-rich phases are likely related to specific biogeochemical reactions responding to Zn incorporation. These findings support the relevant role of biominerals in acting as critical detoxification sinks within certain organisms to remove potentially toxic elements from their immediate environments (Carney et al. 2007).

We were not able to assess if the Zn-independent phases were produced by the investigated mollusks, exposed to high availability of Zn, as a by-product of the molecular machinery during the Ca-carbonate synthesis or due to specific tolerance mechanisms. We cannot conclude that Zn-independent phases can also be formed in bivalve shells having a Zn content lower than 30 ppm due to the weakness of the XANES signal, which would require an experimental setup specifically addressed to ultradiluted compounds.

Future studies should comprise (i) combined analysis of the soft tissues and shells to observe if potential correlations between the metal content and Zn coordination environment occur, and (ii) XAS microbeam analyses at a micro-nanoscale on shell cross-sections to clarify the chemical environment of Zn within the shells of these marine bivalves and to understand the mechanisms involved in Zn incorporation.

Acknowledgments The authors acknowledge the CERIC-ERIC Consortium (grant numbers: 20152041, 20162061, 20167045) for the access to experimental facilities and financial support and the Romanian Ministry of Education (through the Core Program, Project PN16-480102). XAFS (Elettra) 20160254 beamtime, Diamond SP 16496 beamtime, and grant are acknowledged. The research leading to this result has been supported by the project CALIPSOplus under the Grant Agreement 730872 from the EU Framework Programme for Research and Innovation HORIZON 2020. GDG and DM acknowledge RAS (grant number: E58C16000080003) and RAS/FBS (grant number: F72F16003080002). The Grant of Excellence Departments, MIUR (ARTICOLO 1, COMMI 314–337 LEGGE 232/2016), is gratefully acknowledged. We also thank three anonymous Journal Reviewers for their excellent constructive comments.

References

Adediran GA, Ngwenya BT, Mosselmans JFW, Heal KV (2016) Bacteria-zinc co-localization implicates enhanced synthesis of cysteine-rich peptides in zinc detoxification when Brassica juncea

is inoculated with Rhizobium leguminosarum. New Phytol 209: 280–293. https://doi.org/10.1111/nph.13588

Ahmad A, Mukherjee P, Mandal D, Senapati S, Khan MI, Kumar R, Sastry M (2002) Enzyme mediated extracellular synthesis of CdS nanoparticles by the fungus, Fusarium oxysporum. J Am Chem Soc 124:12108–12109. https://doi.org/10.1021/ja027296o

Amoozadeh E, Malek M, Rashidinejad R, Nabavi S, Karbassi M, Ghayoumi R, Ghorbanzadeh-Zafarani G, Salehi H, Sures B (2014) Marine organisms as heavy metal bioindicators in the Persian Gulf and the Gulf of Oman. Environ Sci Pollut Res 21:2386–2395. https://doi.org/10.1007/s11356-013-1890-8

Andral B, Galgani F, Tomasino C, Bouchoucha M, Blottiere C, Scarpato A, Benedicto J, Deudero S, Calvo M, Cento A, Benbrahim S, Boulahdid M, Sammari C (2011) Chemical contamination baseline in the Western Basin of the Mediterranean Sea based on transplanted mussels. Arch Environ Contam Toxicol 61:261–271. https://doi.org/10.1007/s00244-010-9599-x

Apitz SE, Degetto S, Cantaluppi C (2009) The use of statistical methods to separate natural background and anthropogenic concentrations of trace elements in radio-chronologically selected surface sediments of the Venice lagoon. Mar Pollut Bull 58:402–414. https://doi.org/10.1016/j.marpolbul.2008.10.007

Arfaeinia H, Nabipour I, Ostovar A, Asadgol Z, Abuee E, Keshtkar M, Dobaradaran S (2016) Assessment of sediment quality based on acid-volatile sulfide and simultaneously extracted metals in heavily industrialized area of Asaluyeh, Persian gulf: concentrations, spatial distributions, and sediment bioavailability/toxicity. Environ Sci Pollut Res 23:9871–9890. https://doi.org/10.1007/s11356-016-6189-0

Arivalagan J, Yarra T, Marie B, Sleight VA, Duvernois-Berthet E, Clark MS, Marie A, Berland S (2017) Insights from the shell proteome: biomineralization to adaptation. Mol Biol Evol 34:66–77. https://doi.org/10.1093/molbev/msw219

Atzori G, Aru V, Marincola FC et al (2018) Sediments distribution of trace metals in a coastal lagoon (southern Sardinia, Mediterranean Sea): assessment of contamination and ecological risk. Chem Ecol 34:727–746. https://doi.org/10.6084/m9.figshare.6714137.v1

Bechstädt T, Boni M (1994) Sedimentological, stratigraphical and ore deposits field guide of the autochthonous Cambro-Ordovician of southwestern Sardinia: Servizio Geologico d'Italia Memorie Descritive carta Geologica d'Italia, v. XLVIII, 434 p

Benfatto M, Meneghini C (2014) A close look into the low energy region of the XAS spectra: the XANES region. In: Synchrotron radiation, basic, methods and applications. Mobilio, S., Boscherini, F., Meneghini, C., Springer-Verlag, Berlin, pp 213–240

Bilgin M, Uluturhan-Suzer E (2017) Assessment of trace metal concentrations and human health risk in clam (Tapes decussatus) and mussel (Mytilus galloprovincialis) from the Homa lagoon (eastern Aegean Sea). Environ Sci Pollut Res 24:4174–4184. https://doi.org/10.1007/s11356-016-8163-2

Boening DW (1999) An evaluation of bivalves as biomonitors of heavy metals pollution in marine waters. Environ Monit Assess 55:459–470. https://doi.org/10.1023/A:1005995217901

Boni M, Gilg HA, Aversa G, Balassone G (2003) The "calamine" of Southwest Sardinia: geology, mineralogy, and stable isotope geochemistry of supergene Zn mineralization. Econ Geol 98:731–748. https://doi.org/10.2113/gsecongeo.98.4.731

Brown BE (1982) The form and function of metal-containing granules in invertebrate tissues. Biol Rev 57:621–625. https://doi.org/10.1111/j.1469-185X.1982.tb00375.x

Brown ME, Kowalewski M, Neves RJ, Cherry DS, Schreiber ME (2005) Freshwater mussel shells as environmental chronicles: geochemical and taphonomic signatures of mercury-related extirpations in the north fork Holston River, Virginia. Environ Sci Technol 39:1455–1462. https://doi.org/10.1021/es048573p

Caldelas C, Weiss DJ (2017) Zinc homeostasis and isotopic fractionation in plants: a review. Plant Soil 411:17–46. https://doi.org/10.1007/s11104-016-3146-0

Cariou E, Guivel C, La C et al (2017) Lead accumulation in oyster shells, a potential tool for environmental monitoring. Mar Pollut Bull 125: 19–29. https://doi.org/10.1016/j.marpolbul.2017.07.075

Carney CK, Harry SR, Sewell SL (2007) Detoxification biominerals. In: Biomineralization I. Topics in current chemistry. Naka K., Springer, Berlin, Heidelberg, pp 155–185

Carroll M, Romanek CS (2008) Shell layer variation in trace element concentration for the freshwater bivalve Elliptio complanata. Geo-Mar Lett 28:369–381. https://doi.org/10.1007/s00367-008-0117-3

Castillo-Michel HA, Larue C, Pradas del Real AE et al (2017) Practical review on the use of synchrotron based micro- and nano-x-ray fluorescence mapping and x-ray absorption spectroscopy to investigate the interactions between plants and engineered nanomaterials. Plant Physiol Biochem 110:13–32. https://doi.org/10.1016/j.plaphy.2016.07.018

Checa A (2000) A new model for periostracum and shell formation in Unionidae (Bivalvia, Mollusca). Tissue Cell 32:405–416. https://doi.org/10.1054/tice.2000.0129

Cherchi A, Buosi C, Zuddas P, De Giudici G (2012) Bioerosion by microbial euendoliths in benthic foraminifera from heavy metal-polluted coastal environments of Portovesme (South-Western Sardinia, Italy). Biogeosciences 9:4607–4620. https://doi.org/10.5194/bg-9-4607-2012

Cidu R, Biddau R, Fanfani L (2009) Impact of past mining activity on the quality of groundwater in SW Sardinia (Italy). J Geochem Explor 100:125–132. https://doi.org/10.1016/j.gexplo.2008.02.003

Cidu R, Medas D, Di Palma M (2007) The Fluminese mining district (SW Sardinia, Italy): impact of the past lead-zinc exploitation on aquatic environment. R. Cidu & F. Frau, Mako Edizioni, Cagliari, pp 47–51

Conners DE, Westerfield SM, Feyko A, Black MC (1999) Lead accumulation in soft tissues and shells of Asiatic clams (Corbicula fluminea). In: Proceedings of the Georgia water resources conference. Hatcher, K. J., Athens, GA: University of Georgia., pp 597–600

Coombs J, George SG (1978) Mechanisms of immobilization and detoxification of metals in marine organisms. In: Physiology and behavior of marine organism. D.S. McLusky and A.J. Berry, Pergamon Press, Oxford, pp 179–185

Cunningham DP, Lundie LLJ (1993) Precipitation of cadmium by Clostridium thermoaceticum. Appl Environ Microbiol 59:7–14

De Giudici G, Lattanzi P, Medas D (2014a) Synchrotron radiation and environmental sciences. In: Synchrotron radiation. Mobilio, S., Boscherini, F., Meneghini, C., Springer-Verlag Berlin Heidelberg, pp 661–676

De Giudici G, Medas D, Cidu R et al (2018a) Application of hydrologic-tracer techniques to the Casargiu adit and Rio Irvi (SW-Sardinia, Italy): using enhanced natural attenuation to reduce extreme metal loads. Appl Geochem 96:42–54. https://doi.org/10.1016/j.apgeochem.2018.06.004

De Giudici G, Medas D, Meneghini C et al (2015) Microscopic biomineralization processes and Zn bioavailability: a synchrotron-based investigation of Pistacia lentiscus L. roots. Environ Sci Pollut Res Int 22:19352–19361. https://doi.org/10.1007/s11356-015-4808-9

De Giudici G, Meneghini C, Medas D et al (2018b) Coordination environment of Zn in foraminifera Elphidium aculeatum and Quinqueloculina seminula shells from a polluted site. Chem Geol 477:100–111. https://doi.org/10.1016/j.chemgeo.2017.12.009

De Giudici G, Pusceddu C, Medas D et al (2017) The role of natural biogeochemical barriers in limiting metal loading to a stream affected by mine drainage. Appl Geochem 76:124–135. https://doi.org/10.1016/j.apgeochem.2016.11.020

De Giudici G, Wanty RB, Podda F et al (2014b) Quantifying biomineralization of zinc in the rio Naracauli (Sardinia, Italy), using a tracer

injection and synoptic sampling. Chem Geol 384:110–119. https://doi.org/10.1016/j.chemgeo.2014.07.002

Deb SC, Fukushima T (1999) Metals in aquatic ecosystems: mechanisms of uptake, accumulation and release-ecotoxicological perspectives. Int J Environ Sci Technol 56:385–417. https://doi.org/10.1080/00207239908711212

Di Cicco AD, Aquilanti G, Minicucci M et al (2009) Novel XAFS capabilities at ELETTRA synchrotron light source. J Phys Conf Ser 190: 012043

Dobaradaran S, Nabipour I, Saeedi R, Ostovar A, Khorsand M, Khajeahmadi N, Hayati R, Keshtkar M (2017) Association of metals (Cd, Fe, As, Ni, Cu, Zn and Mn) with cigarette butts in northern part of the Persian Gulf. Tob Control 26:461–463. https://doi.org/10.1136/tobaccocontrol-2016-052931

Dobaradaran S, Schmidt TC, Nabipour I, Ostovar A, Raeisi A, Saeedi R, Khorsand M, Khajeahmadi N, Keshtkar M (2018a) Cigarette butts abundance and association of mercury and lead along the Persian Gulf beach: an initial investigation. Environ Sci Pollut Res 25:5465–5473. https://doi.org/10.1007/s11356-017-0676-9

Dobaradaran S, Soleimani F, Nabipour I, Saeedi R, Mohammadi MJ (2018b) Heavy metal levels of ballast waters in commercial ships entering Bushehr port along the Persian Gulf. Mar Pollut Bull 126: 74–76. https://doi.org/10.1016/j.marpolbul.2017.10.094

Faggio C, Tsarpali V, Dailianis S (2018) Mussel digestive gland as a model tissue for assessing xenobiotics: an overview. Sci Total Environ 636:220–229. https://doi.org/10.1016/j.scitotenv.2018.04.264

Foster LC, Allison N, Finch AA, Andersson C (2009) Strontium distribution in the shell of the aragonite bivalve Arctica islandica. Geochem Geophys 10:Q03003. https://doi.org/10.1029/2007GC001915

Foster LC, Finch AA, Allison N, Andersson C, Clarke LJ (2008) Mg in aragonitic bivalve shells: seasonal variations and mode of incorporation in Arctica islandica. Chem Geol 254:113–119. https://doi.org/10.1016/j.chemgeo.2008.06.007

Frau F, Medas D, Da Pelo S et al (2015) Environmental effects on the aquatic system and metal discharge to the Mediterranean Sea from a near-neutral zinc-ferrous sulfate mine drainage. Water Air Soil Pollut 226:55. https://doi.org/10.1007/s11270-015-2339-0

George SG, Pirie BJS, Cheyne AR, Coombs TL, Grant PT (1978) Detoxication of metals by marine bivalves: an ultrastructural study of the compartmentation of copper and zinc in the oyster Ostrea edulis. Mar Biol 45:147–156. https://doi.org/10.1007/BF00390550

Géret F, Jouan A, Turpin V et al (2002) Influence of metal exposure on metallothionein synthesis and lipid peroxidation in two bivalve mollusks: the oyster (Crassostrea gigas) and the mussel (Mytilus edulis). Aquat Living Resour 15:61–66. https://doi.org/10.1016/S0990-7440(01)01147-0

Gianoncelli A, Kaulich B, Alberti R, Klatka T, Longoni A, de Marco A, Marcello A, Kiskinova M (2009) Simultaneous soft x-ray transmission and emission microscopy. Nucl Instrum Methods Phys Res A 608:195–198. https://doi.org/10.1016/j.nima.2009.06.035

Gianoncelli A, Kourousias G, Altissimo M et al (2016b) Combining multiple imaging techniques at the TwinMic X-ray microscopy beamline. AIP Conference Proceedings 1764:030002. https://doi.org/10.1063/1.4961136

Gianoncelli A, Kourousias G, Merolle L, Altissimo M, Bianco A (2016a) Current status of the TwinMic beamline at Elettra: a soft x-ray transmission and emission microscopy station. J Synchrotron Radiat 23: 1526–1537. https://doi.org/10.1107/S1600577516014405

Gianoncelli A, Kourousias G, Stolfa A, Kaulich B (2013) Recent developments at the TwinMic beamline at ELETTRA: an 8 SDD detector setup for low energy x-ray fluorescence. J Phys Conf Ser 425: 182001

Gianoncelli A, Morrison GR, Kaulich B, Bacescu D, Kovac J (2006) A fast readout CCD camera system for scanning x-ray microscopy. Appl Phys Lett 89:251117–251119. https://doi.org/10.1063/1.2422908

Gillikin D, Lorrain A, Navez J et al (2005) Strong biological controls on Sr/Ca ratios in aragonitic marine bivalve shells. Geochem Geophys 6. https://doi.org/10.1029/2004GC000874

Guo X, Feng C (2018) Biological toxicity response of Asian clam (Corbicula fluminea) to pollutants in surface water and sediment. Sci Total Environ 631–632:56–70. https://doi.org/10.1016/j.scitotenv.2018.03.019

Hahn S, Rodolfo-Metalpa R, Griesshaber E, Schmahl WW, Buhl D, Hall-Spencer JM, Baggini C, Fehr KT, Immenhauser A (2012) Marine bivalve shell geochemistry and ultrastructure from modern low pH environments: environmental effect versus experimental bias. Biogeosciences 9:1897–1914. https://doi.org/10.5194/bg-9-1897-2012

Holmes JD, Smith PR, Evans-Gowing R, Richardson DJ, Russell DA, Sodeau JR (1995) Energy-dispersive x-ray analysis of the extracellular cadmium sulfide crystallites of Klebsiella aerogenes. Arch Microbiol 163:143–147. https://doi.org/10.1007/BF00381789

Huanxin W, Lejun Z, Presley BJ (2000) Bioaccumulation of heavy metals in oyster (Crassostrea virginica) tissue and shell. Environ Geol 39: 1216–1226. https://doi.org/10.1007/s002540000110

Jou L-J, Chen B-C, Chen W-Y, Liao C-M (2016) Sensory determinants of valve rhythm dynamics provide in situ biodetection of copper in aquatic environments. Environ Sci Pollut Res Int 23:5374–5389. https://doi.org/10.1007/s11356-015-5735-5

Karbasdehi VN, Dobaradaran S, Nabipour I, Ostovar A, Vazirizadeh A, Ravanipour M, Nazmara S, Keshtkar M, Mirahmadi R, Noorinezhad M (2016a) A new bioindicator, shell of Trachycardium lacunosum, and sediment samples to monitors metals (Al, Zn, Fe, Mn, Ni, V, Co, Cr and Cu) in marine environment: the Persian Gulf as a case. J Environ Health Sci Eng 14:16. https://doi.org/10.1186/s40201-016-0260-0

Karbasdehi VN, Dobaradaran S, Nabipour I, Arfaeinia H, Mirahmadi R, Keshtkar M (2016b) Data on metal contents (As, Ag, Sr, Sn, Sb, and Mo) in sediments and shells of Trachycardium lacunosum in the northern part of the Persian Gulf. Data in Brief 8:966–971. https://doi.org/10.1016/j.dib.2016.06.065

Kastner M (1999) Oceanic minerals: their origin, nature of their environment, and significance. Proc Natl Acad Sci U S A 96:3380–3387. https://doi.org/10.1073/pnas.96.7.3380

Kaulich B, Bacescu D, Susini J, et al (2006) Proceeding 8th international conference x-ray microscopy IPAP Conf. Series. S. Aoki, Y. Kagoshima, Y. Suzuki, p 22

Kennedy WJ, Taylor JD, Hall A (2008) Environmental and biological controls on bivalve shell mineralogy. Biol Rev 44:499–530. https://doi.org/10.1111/j.1469-185X.1969.tb00610.x

Klein RT, Lohmann KC, Thayer CW (1996) SrCa and 13C12C ratios in skeletal calcite of Mytilus trossulus: covariation with metabolic rate, salinity, and carbon isotopic composition of seawater. Geochim Cosmochim Acta 60:4207–4221. https://doi.org/10.1016/S0016-7037(96)00232-3

Koide M, Lee DS, Goldberg ED (1982) Metal and transuranic records in mussel shells, byssal threads and tissues. Estuar Coast Shelf Sci 15: 679–695

Kong Y, Jing G, Yan Z, Li C, Gong N, Zhu F, Li D, Zhang Y, Zheng G, Wang H, Xie L, Zhang R (2009) Cloning and characterization of Prisilkin-39, a novel matrix protein serving a dual role in the prismatic layer formation from the oyster Pinctada fucata. J Biol Chem 284:10841–10854. https://doi.org/10.1074/jbc.M808357200

Kucuksezgin F, Pazi I, Yucel-Gier G, Akcali B, Galgani F (2013) Monitoring of heavy metal and organic compound levels along the eastern Aegean coast with transplanted mussels. Chemosphere 93: 1511–1518. https://doi.org/10.1016/j.chemosphere.2013.07.058

Lafabrie C, Pergent G, Kantin R, Pergent-Martini C, Gonzalez JL (2007) Trace metals assessment in water, sediment, mussel and seagrass

species—validation of the use of Posidonia oceanica as a metal biomonitor. Chemosphere 68:2033–2039. https://doi.org/10.1016/j.chemosphere.2007.02.039

Lerotic M, Mak R, Wirick S, Meirer F, Jacobsen C (2014) MANTiS: a program for the analysis of x-ray spectromicroscopy data. J Synchrotron Radiat 21:1206–1212. https://doi.org/10.1107/S1600577514013964

Lopes-Lima M, Freitas S, Pereira L, Gouveia E, Hinzmann M, Checa A, Machado J (2012) Ionic regulation and shell mineralization in the bivalve Anodonta cygnea (swan mussel) following heavy-metal exposure. Can J Zool 90:267–283. https://doi.org/10.1139/z11-129

Lowenstam HA, Weiner S (1989) On biomineralization. Oxford University Press, New York

Luo L, Zhang S (2010) Applications of synchrotron-based x-ray techniques in environmental science. Sci China Chem 53:2529–2538. https://doi.org/10.1007/s11426-010-4085-x

Lutz RA (2004) Bivalve molluscs: biology, ecology and culture by Elizabeth Gosling the quarterly review of biology 79:317–317. doi: https://doi.org/10.1086/425799

Marcello A, Pretti S, Valera P, et al (2004) Metallogeny in Sardinia (Italy): from the Cambrian to the tertiary. In: 32nd international geological congress, APAT 4, 14–36, Firenze., mem. Descr. Carta Geol. d'It. Guerrieri L., Rischia I., Serva L

Marin F, Roy NL, Marie B (2012) The formation and mineralization of mollusk shell. Front Biosci 4:1099–1125

Medas D, Cidu R, De Giudici G, Podda F (2013) Geochemistry of rare earth elements in water and solid materials at abandoned mines in SW Sardinia (Italy). J Geochem Explor 133:149–159

Medas D, De Giudici G, Casu MA et al (2015) Microscopic processes ruling the bioavailability of Zn to roots of euphorbia pithyusa L. pioneer plant. Environ Sci Technol 49:1400–1408. https://doi.org/10.1021/es503842w

Medas D, De Giudici G, Podda F et al (2014a) Apparent energy of hydrated biomineral surface and apparent solubility constant: an investigation of hydrozincite. Geochim Cosmochim Acta 140:349–364. https://doi.org/10.1016/j.gca.2014.05.019

Medas D, De Giudici G, Pusceddu C et al (2017b) Impact of Zn excess on biomineralization processes in Juncus acutus grown in mine polluted sites. J Hazard Mater. https://doi.org/10.1016/j.jhazmat.2017.08.031

Medas D, Lattanzi P, Podda F, Meneghini C, Trapananti A, Sprocati A, Casu MA, Musu E, De Giudici G (2014b) The amorphous Zn biomineralization at Naracauli stream, Sardinia: electron microscopy and X-ray absorption spectroscopy. Environ Sci Pollut Res 21(11):6775–6782

Medas D, Meneghini C, Podda F, Floris C, Casu M, Casu MA, Musu E, de Giudici G (2018) Structure of low-order hemimorphite produced in a Zn-rich environment by cyanobacterium Leptolingbya frigida. Am Mineral 103:711–719. https://doi.org/10.2138/am-2018-6128

Medas D, Podda F, Meneghini C, De Giudici G (2017a) Stability of biological and inorganic hemimorphite: implications for hemimorphite precipitation in non-sulfide Zn deposits. Ore Geol Rev 89:808–821. https://doi.org/10.1016/j.oregeorev.2017.07.015

Meneghini C, Bardelli F, Mobilio S (2012) ESTRA-FitEXA: a software package for EXAFS data analysis. Nucl Instrum Methods Phys Res B 285:153–157. https://doi.org/10.1016/j.nimb.2012.05.027

Meneghini C, Di Matteo S, Monesi C et al (2005) Structural dichroism in the antiferromagnetic insulating phase of V2O3. Phys Rev B 72:033111. https://doi.org/10.1103/PhysRevB.72.033111

Morelli G, Rimondi V, Benvenuti M, Medas D, Costagliola P, Gasparon M (2017) Experimental simulation of arsenic desorption from quaternary aquifer sediments following sea water intrusion. Appl Geochem 87:176–187. https://doi.org/10.1016/j.apgeochem.2017.10.024

Morrison GR, Gianoncelli A, Kaulich B, et al (2006) A fast readout CCD system for configured-detector imaging in STXM. In: Conf. Proc. Ser. IPAP. pp 277–379

Moschino V, Schintu M, Marrucci A, Marras B, Nesto N, da Ros L (2017) An ecotoxicological approach to evaluate the effects of tourism impacts in the marine protected area of La Maddalena (Sardinia, Italy). Mar Pollut Bull 122:306–315. https://doi.org/10.1016/j.marpolbul.2017.06.062

Moura G, Guedes R, Machado J (1999) The extracellular mineral concretions in Anodonta cygnea (L.): different types and manganese exposure-caused changes. J Shellfish Res 18:645–650

Numpy https://docs.scipy.org/doc/numpy-1.14.0/reference/generated/numpy.corrcoef.html - Copyright 2008-2009, The Scipy community. Last updated on May 11, 2014

Pietrzak J, Bates J, Scott R (1976) Constituents of unionoid extrapalial fluid. II pH and metal ion composition. Hydrobiologia 50:89–93

Podda F, Medas D, De Giudici G, Ryszka P, Wolowski K, Turnau K (2014) Zn biomineralization processes and microbial biofilm in a metal-rich stream (Naracauli, Sardinia). Environ Sci Pollut Res 21(11):6793–6808

RAS (2008) Regione Autonoma della Sardegna - Piano Regionale di gestione dei rifiuti - Piano di bonifica siti inquinati

Romano E, De Giudici G, Bergamin L et al (2017) The marine sedimentary record of natural and anthropogenic contribution from the Sulcis-Iglesiente mining district (Sardinia, Italy). Mar Pollut Bull 122:331–343. https://doi.org/10.1016/j.marpolbul.2017.06.070

Rosenberg GD, Hughes WW (1991) A metabolic model for the determination of shell composition in the bivalve mollusc, Mytilus edulis. Lethaia 24:83–96. https://doi.org/10.1111/j.1502-3931.1991.tb01182.x

Rzymski P, Niedzielski P, Klimaszyk P, Poniedziałek B (2014) Bioaccumulation of selected metals in bivalves (Unionidae) and Phragmites australis inhabiting a municipal water reservoir. Environ Monit Assess 186:3199–3212. https://doi.org/10.1007/s10661-013-3610-8

Salvi G, Buosi C, Arbulla D et al (2015) Ostracoda and foraminifera response to a contaminated environment: the case of the ex-military arsenal of the la Maddalena harbour (Sardinia, Italy). Micropaleontol 61:115–133

Sarmiento AM, Bonnail E, Nieto JM, DelValls A (2016) Bioavailability and toxicity of metals from a contaminated sediment by acid mine drainage: linking exposure-response relationships of the freshwater bivalve Corbicula fluminea to contaminated sediment. Environ Sci Pollut Res Int 23:22957–22967. https://doi.org/10.1007/s11356-016-7464-9

Schintu M, Durante L, Maccioni A, Meloni P, Degetto S, Contu A (2008) Measurement of environmental trace-metal levels in Mediterranean coastal areas with transplanted mussels and DGT techniques. Mar Pollut Bull 57:832–837. https://doi.org/10.1016/j.marpolbul.2008.02.038

Scipy https://docs.scipy.org/doc/scipy-0.14.0/reference/generated/scipy.stats.spearmanr.html - Copyright 2008-2009, The Scipy community. Last updated on May 11, 2014

Sforzini S, Oliveri C, Orrù A, Chessa G, Pacchioni B, Millino C, Jha AN, Viarengo A, Banni M (2018) Application of a new targeted low density microarray and conventional biomarkers to evaluate the health status of marine mussels: a field study in Sardinian coast, Italy. Sci Total Environ 628–629:319–328. https://doi.org/10.1016/j.scitotenv.2018.01.293

Simkiss K, Mason AZ (1983) 4 - Metal ions: metabolic and toxic effects 1 A2 - Hochachka, Peter W. In: The Mollusca. Academic Press, San Diego, pp 101–164

Soldati AL, Jacob DE, Glatzel P, Swarbrick JC, Geck J (2016) Element substitution by living organisms: the case of manganese in mollusc shell aragonite. Sci Rep 6:22514. https://doi.org/10.1038/srep22514

Solé VA, Papillon E, Cotte M, Walter P, Susini J (2007) A multiplatform code for the analysis of energy-dispersive x-ray fluorescence spectra. Spectrochim Acta Part B At Spectrosc 62:63–68. https://doi.org/10.1016/j.sab.2006.12.002

Soleimani F, Dobaradaran S, Hayati A, Khorsand M, Keshtkar M (2016) Data on metals (Zn, Al, Sr, and Co) and metalloid (As) concentration levels of ballast water in commercial ships entering Bushehr port, along the Persian Gulf. Data in Brief 9:429–432. https://doi.org/10.1016/j.dib.2016.09.017

Stara P, Rizzo R, Tanca GA (1996) Iglesiente-Arburese: Miniere e Minerali. Centrooffset, Siena

Stecher HA, Krantz DE, Lord CJ et al (1996) Profiles of strontium and barium in Mercenaria mercenaria and Spisula solidissima shells. Geochim Cosmochim Ac 60:3445–3456. https://doi.org/10.1016/0016-7037(96)00179-2

Steinhardt J, Butler PG, Carroll ML, Hartley J (2016) The application of long-lived bivalve sclerochronology in environmental baseline monitoring. Front Mar Sci 3:176. https://doi.org/10.3389/fmars.2016.00176

Suzuki M, Murayama E, Inoue H et al (2004) Characterization of prismalin-14, a novel matrix protein from the prismatic layer of the Japanese pearl oyster (Pinctada fucata). Biochem J 382:205–213. https://doi.org/10.1042/BJ20040319

Suzuki M, Sakuda S, Nagasawa H (2007) Identification of chitin in the prismatic layer of the shell and a chitin synthase gene from the Japanese pearl oyster, Pinctada fucata. Biosci Biotechnol Biochem 71:1735–1744

Taylor JD, Kennedy WJ, Hall A (1969) The shell structure and mineralogy of Bivalvia: introduction, nuculacea-trigonacea. Nuculacea-Trigonacea Bull Br Mus 3:1–125

Terzano R, Al Chami Z, Vekemans B et al (2008) Zinc distribution and speciation within rocket plants (Eruca vesicaria L. Cavalieri) grown on a polluted soil amended with compost as determined by XRF microtomography and micro-XANES. J Agric Food Chem 56:3222–3231. https://doi.org/10.1021/jf073304e

Tevesz MJS, Carter JG (1980) Environmental relationships of shell form and structure of Unionacean bivalves. In: Skeletal growth of aquatic organisms. Rhoads D.C., Lutz R., Plenum, New York, pp 295–322

Torchio R, Meneghini C, Mobilio S, Capellini G, Garcia Prieto A, Alonso J, Fdez-Gubieda ML, Turco Liveri V, Longo A, Ruggirello AM, Neisius T (2010) Microstructure and magnetic properties of colloidal cobalt nano-clusters. J Magn Magn Mater 322:3565–3571. https://doi.org/10.1016/j.jmmm.2010.07.008

Tsukamoto D, Sarashina I, Endo K (2004) Structure and expression of an unusually acidic matrix protein of pearl oyster shells. Biochem Biophys Res Commun 320:1175–1180. https://doi.org/10.1016/j.bbrc.2004.06.072

Tynan S, Eggins S, Kinsley L et al (2005) Mussel shells as environmental tracers: an example from the Loveday Basin. Regolith:314–317

Vaughn CC (2018) Ecosystem services provided by freshwater mussels. Hydrobiologia 810:15–27. https://doi.org/10.1007/s10750-017-3139-x

Weiner S, Lowenstam HA, Hood L (1976) Characterization of 80-million-year-old mollusk shell proteins. Proc Natl Acad Sci U S A 73:2541–2545

Wilbur KM, Saleuddin ASM (1983) Shell formation. In: The Mollusca. Saleuddin ASM, Wilbur KM, Academic, New York, pp 235–287

Wong KW, Yap CK, Nulit R, Hamzah MS, Chen SK, Cheng WH, Karami A, al-Shami SA (2017) Effects of anthropogenic activities on the heavy metal levels in the clams and sediments in a tropical river. Environ Sci Pollut Res Int 24:116–134. https://doi.org/10.1007/s11356-016-7951-z

Yan H, Chen J, Xiao J (2014) A review on bivalve shell, a tool for reconstruction of paleo-climate and paleo-environment. Chin J Chem 33:310–315. https://doi.org/10.1007/s11631-014-0692-0

Yao Z, Xia M, Li H, Chen T, Ye Y, Zheng H (2014) Bivalve shell: not an abundant useless waste but a functional and versatile biomaterial. Crit Rev Environ Sci Technol 44:2502–2530. https://doi.org/10.1080/10643389.2013.829763

Yoshimura T, Tamenori Y, Suzuki A, Nakashima R, Iwasaki N, Hasegawa H, Kawahata H (2013) Element profile and chemical environment of sulfur in a giant clam shell: insights from μ-XRF and x-ray absorption near-edge structure. Chem Geol 352:170–175. https://doi.org/10.1016/j.chemgeo.2013.05.035

Zuykov M, Pelletier E, Harper DAT (2013) Bivalve mollusks in metal pollution studies: from bioaccumulation to biomonitoring. Chemosphere 93:201–208. https://doi.org/10.1016/j.chemosphere.2013.05.001